

Electronic and magnetic structure at the Fe/Fe₃O₄ interfaceT. Kida,¹ S. Honda,³ H. Itoh,² and J. Inoue^{1,*}¹*Department of Applied Physics, Nagoya University, Nagoya 464-8603, Japan*²*Department of Pure and Applied Physics, Kansai University, Suita 564-8680, Japan*³*ORDIST Kansai University, Suita 564-8680, Japan*

H. Yanagihara and E. Kita

Institute of Applied Physics, University of Tsukuba, Tsukuba 305-8573, Japan

K. Mibu

Graduate School of Engineering, Nagoya Institute of Technology, Nagoya 466-8555, Japan

(Received 31 January 2011; revised manuscript received 1 July 2011; published 2 September 2011)

The exchange coupling (EC) observed recently in Fe/Fe₃O₄(001) junctions is comparable in magnitude to that in Co/Ru/Co trilayers and has potential applications in spintronic devices. To clarify the EC mechanism, the electronic and magnetic states of Fe/Fe₃O₄ junctions are calculated via a first-principles method by assuming four structures of bcc Fe layers stacked on Fe₃O₄ (001) layers. We show that the local magnetic moment m of bcc Fe atoms increases at the interface, whereas that of Fe ions at the Fe₃O₄ layer decreases at the interface. The total energy of the junctions is plotted as a function of the distance between Fe and Fe₃O₄ layers. The EC energy between the Fe and Fe₃O₄ layers with flat interfaces is calculated to be two orders of magnitude larger than the experimentally determined EC energy. The large energy is attributed to the interatomic exchange interactions at the interface. To explain the experimental results, we propose a mechanism of EC mediated by the impurity-like states of bcc Fe atoms that possess reversed m at the interface. Frustration effects in the EC between Fe and Fe₃O₄ layers are also discussed.

DOI: [10.1103/PhysRevB.84.104407](https://doi.org/10.1103/PhysRevB.84.104407)

PACS number(s): 75.70.-i, 73.20.-r, 85.70.-w

I. INTRODUCTION

Magnetic junctions composed of more than two thin magnetic layers have provided interesting physics and technological applications in the field of spintronics. Magnetic multilayers consisting of alternate stackings of ferromagnetic and nonmagnetic metals give rise to giant magnetoresistance (GMR)^{1,2} and interlayer exchange coupling (IEC).^{1,3,4} Ferromagnetic tunnel junctions composed of two ferromagnetic layers separated by a thin insulator result in tunnel magnetoresistance (TMR).^{5,6} The direct contact of a ferromagnet (FM) and an antiferromagnet produces the so-called exchange bias (EB)^{7,8} in the magnetization process. These concepts of GMR, IEC, TMR, and EB are essential in spintronic applications.

The search for novel ferromagnetic materials has also provided productive results in the form of high-quality half-metallic FMs in which one spin state is metallic and the other is insulating. Typical examples of half-metals are Heusler alloys and perovskite Mn oxides.⁹⁻¹² Because spin polarization of the density of states (DOS) at the Fermi level is high in half-metals, they are promising in spintronic applications. In fact, tunnel junctions composed of Heusler alloys exhibit high TMR ratios.^{13,14} The magnetite Fe₃O₄—the first ferromagnet ever discovered—was also predicted to be half-metallic by first-principles band calculations.^{15,16} Several attempts were made to use Fe₃O₄ in tunnel junctions aiming at high TMR ratios, but the obtained TMR ratio was not sufficiently high for practical applications.¹⁷⁻²¹ Nevertheless, Fe₃O₄ films attract much interests as a means to explore spin-dependent properties such as the oscillatory spin polarization of epitaxial Fe₃O₄ films on GaAs and polar switching in Fe₃O₄-BiFeO₃ nanocomposite thin films.^{22,23}

Yanagihara *et al.* recently observed exchange coupling (EC) in Fe/MgO/ γ -Fe₂O₃ and Fe/MgO/Fe₃O₄ junctions by using the magnetization and magneto-optical measurements.²⁴⁻²⁶ The coupling is antiferromagnetic, i.e., the Fe and Fe₃O₄ magnetizations align antiparallel to each other. The EC is antiparallel even in Fe/Fe₃O₄ junctions and the EC magnitude (approximately 1.5 erg/cm² in Fe/Fe₃O₄) decays with increasing MgO thickness. This value is similar to the IEC value in Co/Ru/Co trilayers,⁴ and thus Fe/Fe₃O₄ junctions can be used as synthetic antiferromagnets when the magnetizations of the Fe and Fe₃O₄ layers are compensated. It is noted that the EC shows almost no temperature dependence. Fe/Fe₃O₄ junctions may provide a new type of junctions composed of two different strong ferromagnets (FMs), which are distinct from magnetic trilayers and EB systems.

The IEC in ferromagnetic junctions using an insulating spacer has been reported both theoretically and experimentally.²⁷⁻³⁰ Experimental results for Fe/MgO/Fe/Co²⁹ indicate a sign change in the IEC with increasing MgO thickness and a rapid decay in the IEC magnitude with increasing MgO thickness. Results for Fe/MgO/Fe³⁰ showed that the IEC of Fe/MgO/Fe junctions is smaller than that in Fe/MgO/Fe/Co by one order of magnitude and that oxygen vacancy contributes the antiferromagnetic coupling. On the other hand, EC in Fe/MgO/Fe₃O₄ is antiparallel irrespective of the MgO thickness and the EC values are approximately the same as the IEC values in Fe/MgO/Fe/Co with 0.5–0.9 nm MgO thickness. It is therefore expected that the oxygen deficiency may have an influence also on EC in Fe/MgO/Fe₃O₄ junctions with finite MgO thickness. However, it is rather surprising that a direct contact between two metallic FMs gives

rise to antiparallel EC with a magnitude similar to the IEC in Co/Ru/Co trilayers.

The mechanism behind antiparallel magnetization alignment in Fe and Fe₃O₄ is unclear, and the electronic and magnetic structures of the Fe/Fe₃O₄ and Fe/MgO/Fe₃O₄ junctions are not yet amply studied. The few experimental studies that exist report that the surface of Fe₃O₄(001) has a ($\sqrt{2} \times \sqrt{2}$)45° structure called the modified B(Fe) layer.^{31–33} To explain the mechanism behind EC in Fe/Fe₃O₄ and Fe/MgO/Fe₃O₄ junctions, both theoretical and experimental studies are extremely desirable. In the present study, we perform first-principles band calculations for clean Fe/Fe₃O₄(001) junctions to clarify the electronic and magnetic structures at the interface. We also calculate the total energy of junctions with parallel (P) and antiparallel (AP) alignment of Fe and Fe₃O₄ magnetizations as a function of the interlayer distance between the Fe and Fe₃O₄ layers. We define the difference $E_{AP} - E_P \equiv \Delta E$ between the lowest energies in P and AP alignments as the EC energy and observe that ΔE is larger than the experimental values by two orders of magnitude. The large calculated EC is attributed to an EC between the local magnetic moments at the interface. To explain the experimental results, we propose an extrinsic mechanism for the AP alignment that is mediated by impurity-like states of Fe atoms at the interface.

The bulk Fe₃O₄ forms a cubic lattice at room temperature and transforms to a charge-ordered monoclinic lattice below the so-called Verwey temperature (~ 120 K).^{34–36} Thus far many first-principles band calculations have been performed for bulk Fe₃O₄ with cubic, monoclinic as well as orthorhombic lattice structures.^{15,16,37–43} Recent first-principles calculations that include self-interaction corrections^{42,43} indicate that Fe₃O₄ is indeed half-metallic; this result is consistent with previous ones.^{15,16} A suitable choice for the so-called U parameter in the local spin density approximation (LSDA) + U method gives similar results. The generalized gradient approximation (GGA) + U method adopted to calculate the electronic structure with the monoclinic lattice reproduced the observed charge-ordered state.^{40,41} In the present work, we use the latter method for Fe/Fe₃O₄ junctions and adopt a supercell that includes three bcc Fe atomic layers and four Fe₃O₄ atomic layers. Details of the method used and of the contact structures are presented in the next section. In Sec. III, we present results for the local DOS, local Fe moments in bcc Fe and Fe₃O₄ layers, and the total energy calculated for clean interfaces. Because the atomistic structures at the interface are unknown, we also perform calculations with the spatial relaxation of atomic sites and the direction of magnetic moments at the interface. Calculations using several values of U will also be performed. In Sec. IV, we compare the calculated and experimental results and discuss possible mechanisms for the observed EC. We also discuss magnetic states at the interface from the viewpoint of the recently reported Mössbauer measurements.⁴⁴ Concluding remarks are presented in the final section.

II. METHOD OF CALCULATION AND JUNCTION STRUCTURES

Fe₃O₄ is an inverse spinel ferrite, in which Fe ions exist on tetrahedral sites (called A-sites) surrounded by four O ions

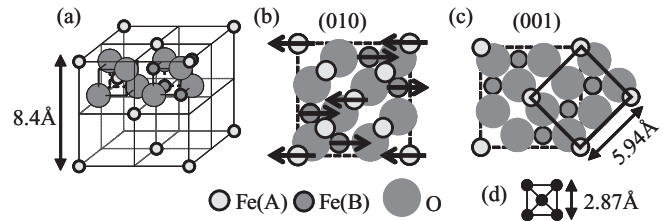


FIG. 1. (a) Lattice structure of spinel ferrites, (b) atomic arrangement on (010) plane, (c) atomic arrangement on (001) plane, where the square with solid lines denotes the $p(1 \times 1)$ structure, and (d) bcc Fe lattice.

or on octahedral sites (B-sites) surrounded by six O ions. The valence of A-site Fe ions is 3+ and that of B-site Fe ions is either 3+ or 2+. Fe₃O₄ is a metal with a resistivity $\rho \sim 4 \times 10^{-3} \Omega \text{ cm}$ at room temperature. Because the observed EC in Fe/Fe₃O₄ shows almost no temperature dependence, we adopt the cubic lattice structure for Fe₃O₄. The lattice structure of Fe₃O₄ is shown in Fig. 1(a). Because the magnetic moments of A-site Fe (hereafter denoted as A-Fe) are antiparallel to those of B-site Fe (B-Fe) and the number of A-Fe sites is half that of B-Fe sites, it can be said Fe₃O₄ is a ferrimagnet with a total magnetic moment $4 \mu_B/\text{Fe}_3\text{O}_4$.

The structure of Fe₃O₄ in the [001] direction [Fig. 1(b)] consists of stacked layers alternating between those that contain only A-Fe ions and those in which B-Fe ions and O ions coexist. The former and latter layers are hereafter called A-Fe and B-Fe layers, respectively. The charge distribution on each layer is not compensated.

The junction structures used in the calculations are determined via the following procedure. An Fe₃O₄ (001) layer may be subject to either an A-Fe layer or a B-Fe layer termination. Examples of B-Fe and A-Fe layer terminations are shown in Figs. 2(a) and 2(b), respectively. We assume that the bcc Fe layer is epitaxially stacked on A-Fe or B-Fe layers and that the modified B-Fe structure reported previously^{31–33} may disappear because of the deposition of the bcc Fe layer. Three plausible structures of a bcc Fe layer commensurate to A-Fe and B-Fe terminations are shown in Figs. 2(c)–2(e). In the figures, solid and broken lines indicate the first and second

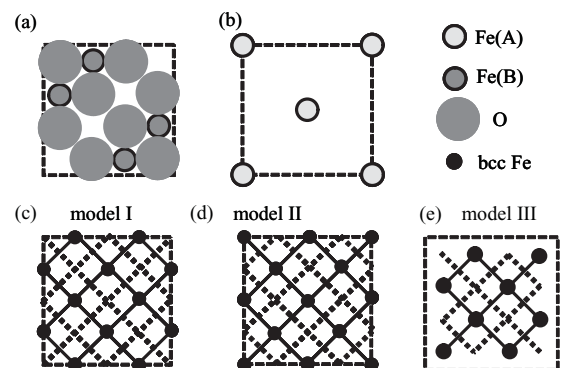


FIG. 2. Atomic arrangement of (a) B-Fe layer and (b) A-Fe layer. (c)–(e) Possible structures of bcc Fe lattice on Fe₃O₄ (001). Solid and broken lines in bcc Fe lattice show the first and second atomic layer, respectively, on Fe₃O₄.

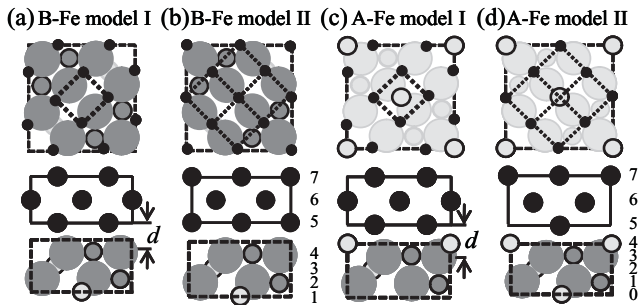


FIG. 3. Junction structures (unit cells) used in the calculation; upper (lower) panels show the top (side) view. (a) Model I of bcc Fe lattice with B-Fe layer termination, (b) model II with B-Fe layer termination, (c) model I with A-Fe layer termination, and (d) model II with A-Fe layer termination. Numbering of atomic layers is also presented.

atomic layer in the bcc Fe layer, respectively. We refer to these structures as models I, II, and III.

In the stacking of model III, shown in Fig. 2(e), Fe atoms on the first atomic layer of the bcc Fe layer may exist in the open space of the B-Fe layer in Fe_3O_4 , but those in the second atomic layer exist immediately above the O sites, which have large ionic radii, resulting in short atomic distances between Fe atoms and O ions. Therefore we omit stacking model III and deal with four junction structures that include A-Fe or B-Fe terminations with commensurate stacking of models I or II, as shown in Fig. 3.

The unit cell used in the calculation contains three atomic layers of bcc Fe and four atomic layers of Fe_3O_4 with a vacuum layer above bcc Fe layer. The cross section of the unit cell on the (001) plane is a $p(1 \times 1)$ structure with 5.95 Å sides as shown in Fig. 1(c). Because the lattice constant of bcc Fe is 2.87 Å [see Fig. 1(d)], there is a minor mismatch in the lattice constants between the bcc Fe and Fe_3O_4 layers. We neglect this small lattice mismatch, and assume that the lattice constant of the cross section is 2.87×2 Å. A unit cell comprises 26 atoms; 12 Fe atoms in the bcc Fe layer, 6 Fe, and 8 O atoms in the Fe_3O_4 layer in the junction structures, except for the A-Fe model II. Because the number of bcc Fe atoms in the structure of A-Fe model II structure is 11, we add another A-Fe atom at the bottom of the structure, as shown in Fig. 3(d), such that the total number of Fe atoms in the unit cell is identical to that in other junction structures.

We use the first-principles band calculation provided by the VASP package,⁴⁵ in which the PAW (projected-augment wave) pseudopotential and a spin-polarized GGA-PW (Perdew-Wang) method, which includes a correction of the Coulomb interaction U , are adopted. The cutoff value of the plane waves is 400 eV. We have chosen the value of $U = 4.5$ eV for Fe ions in Fe_3O_4 as adopted by Leonov *et al.*⁴⁰ and Jeng *et al.*⁴¹ The same value of U has been adopted by Antonov *et al.*,^{38,39} in which LSDA + U was adopted. The latter reported that the calculated results of the electronic structure with $U = 4.5$ eV are in good agreement with experimental ones obtained by magneto-optical measurements and give a reasonable value of the energy band gap in the insulating phase at low temperature. We have confirmed that our calculated results of DOS in GGA + U (4.5 eV) are almost the same with those calculated

by Jeng *et al.*, and consistent with those calculated in HSE06⁴⁶ and those calculated by Szotek *et al.*⁴² U is assumed to be zero for Fe atoms in the bcc Fe layer. The k point sampling is (9,9,1). We confirmed that the results converge sufficiently by performing (9,9,3) and (13,13,1) samplings. The position of the O ions is optimized for bulk Fe_3O_4 in the first-principles calculation and the resultant value of the so-called u parameter is 0.3795, which is reasonable when compared to the ideal value 3/8 and the experimental value of 0.379.⁴⁸

The total energy of the junction, the local density of states (DOS) and the local magnetic moments m of atoms or ions are calculated for the P and AP alignments of bcc Fe and Fe_3O_4 magnetizations. The EC energy of the junction is defined by the difference in the total energy between P and AP alignments, $\Delta E = E_{\text{AP}} - E_{\text{P}}$. When $\Delta E > 0$ (< 0), the P (AP) alignment is stable.

III. CALCULATED RESULTS

In this section, we report the results of our calculation for bulk Fe_3O_4 in subsection A, and present the local DOS, m , E_{P} , and E_{AP} calculated for Fe/ Fe_3O_4 junctions with A-Fe and B-Fe layer terminations in subsections B and C, respectively. Section III D presents the results of calculations for structures that allow the atomic position of Fe atoms or ions to be relaxed. Section III E presents results calculated by relaxing the direction of interfacial magnetic moments and by using smaller values of U .

A. Results for bulk Fe_3O_4

The results of the local DOS calculated for A-Fe and B-Fe ions and total DOS per unit cell of Fe_3O_4 are shown in Figs. 4(a)–4(c). The DOS for bcc Fe is also presented in Fig. 4(d). Both majority- and minority-spin states of A-Fe have an energy band gap at the Fermi energy, which proves that A-Fe ions are insulating. The local DOS for B-Fe, however, has finite DOS at the Fermi energy in the minority-spin state, and shows a half-metallic feature. As a result, bulk Fe_3O_4 becomes half-metallic, as shown in Fig. 4(a). Because u varies from its ideal value, several nonequivalent sites exist for A-Fe, B-Fe, and O ions. However, differences in their local DOS due to the nonequivalence of atomic sites are small. The local DOS for Fe ions in Fe_3O_4 is considerably different from the bulk DOS of bcc Fe, shown in Fig. 4(d), because of a strong hybridization between the p orbitals in O ions and d orbitals in Fe ions.

The calculated values of m for A-Fe and B-Fe ions are approximately $-4.1 \mu_{\text{B}}/\text{atom}$ and $3.9\text{--}4.1 \mu_{\text{B}}/\text{atom}$, respectively, and those for O ions are $0.04\text{--}0.05 \mu_{\text{B}}/\text{atom}$. The total moment is $4.0 \mu_{\text{B}}/\text{Fe}_3\text{O}_4$. There is almost no difference in the absolute values of the magnetic moments in A-Fe and B-Fe ions, which is in contrast to those expected in the ionic model. The results, however, are consistent with previous results calculated via the first-principles method.⁴² Experimental values for A-Fe moment were reported to be -3.8 to $-4.2 \mu_{\text{B}}/\text{atom}$.⁴⁷ In addition, the magnetic moment of Fe in bcc Fe is calculated to be $2.24 \mu_{\text{B}}/\text{atom}$.

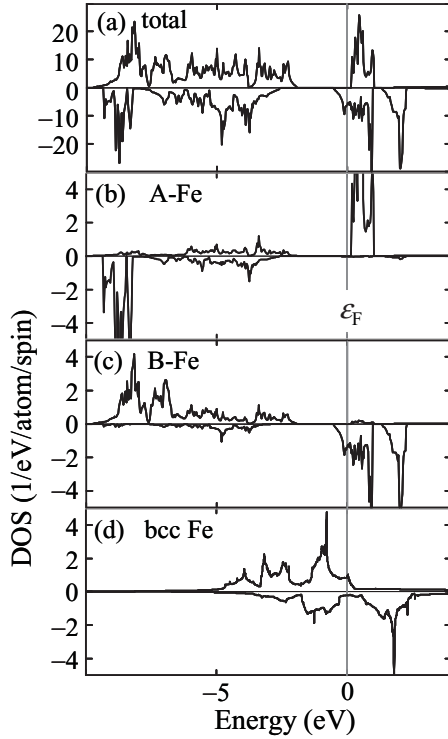


FIG. 4. Calculated results of (a) total DOS of bulk Fe_3O_4 , (b) local DOS of A-Fe ions, (c) local DOS of B-Fe ions, and (d) bulk DOS of bcc Fe.

B. Results for bcc Fe/ Fe_3O_4 junctions with A-Fe layer termination

Calculated results for the local DOS of bcc Fe atoms and A-Fe ions at the interface in the structure of A-Fe model I are shown in Fig. 5 for P and AP alignments. Here, we see that the majority-spin local DOS of bcc Fe atoms is almost saturated, as shown in Figs. 5(a) and 5(b). The energy band gap of Fe-A ions is almost washed away because of band mixing between Fe atoms in bcc Fe and Fe_3O_4 layers.

The calculated values of m for Fe atoms or ions in the unit-cell structures of A-Fe models I and II are presented in Table I. The numbering of the atomic layers in the unit cell

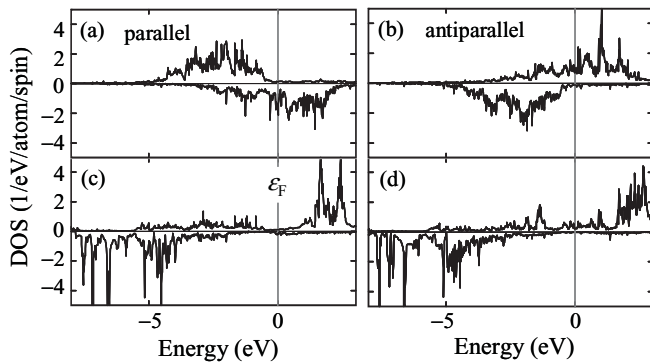


FIG. 5. (a) Local DOS of bcc Fe atoms at interface in parallel (P) alignment and (b) antiparallel (AP) alignment, calculated for A-Fe model I. (c) Calculated results of local DOS for A-Fe ions at the Fe_3O_4 interface in P alignment and (d) AP alignment.

TABLE I. Calculated results for local magnetic moment m on Fe atoms or ions in the unit cell of Fe/ Fe_3O_4 with A-Fe termination. L indicates atomic-layer numbering given in Fig. 3, and I(II)-P(AP) indicate model I(II) with P(AP) alignment of bcc Fe and Fe_3O_4 magnetizations, respectively.

	L	I-P	I-AP	II-P	II-AP
bcc Fe	7	2.928	-2.929	2.894	-2.905
	7	2.920	-2.928	2.966	-2.944
	7	2.920	-2.928	2.959	-2.959
	7	2.928	-2.929	2.905	-2.903
	6	2.323	-2.374	2.424	-2.472
	6	2.312	-2.305	2.420	-2.471
	6	2.323	-2.372	2.420	-2.471
A-Fe	6	2.310	-2.386	2.424	-2.472
	5	2.778	-2.764	2.797	-2.685
	5	2.769	-2.765	2.942	-2.937
	5	2.769	-2.765	2.744	-2.569
	5	2.778	-2.764	-	-
A-Fe	4	-3.403	-3.469	-3.602	-3.566
B-Fe	3	4.012	4.025	3.906	3.815
	3	4.012	4.025	3.906	3.815
A-Fe	2	4.059	-4.070	-4.036	-4.048
B-Fe	1	4.149	4.137	3.725	3.649
	1	4.149	4.137	3.725	3.649
A-Fe	0	-	-	-3.624	-3.625

is presented in Fig. 3. The values of m for A-Fe ions at the interface are reduced to approximately -3.4 to $-3.6\mu_B/\text{atom}$. The reduction of the magnitude may be due to band mixing between bcc Fe and Fe_3O_4 layers. However, the values of m for bcc Fe atoms at the interface increase, thereby reflecting the saturated local DOS of Fe atoms at the interface. The value of m for Fe atoms on the sixth atomic layer is nearly the same as that for bulk Fe, but that on seventh layer increases to approximately $2.9\mu_B/\text{atom}$. The latter results are caused by surface effects because the unit cells shown in Fig. 3 are periodically arranged using a vacuum spacer.

Figure 6 shows the results of the total energy as a function of the interlayer distance d defined in Fig. 3 for A-Fe model I and A-Fe model II. We find several characteristics in Figs. 6(a) and 6(b). A local minimum appears in the total energy with respect to the interlayer distance d . Therefore the assumed structures are at least locally stable. The lowest energy occurs at $d \sim 2.7\text{ \AA}$ in model I. Because the interlayer distance between the A-Fe and B-Fe layer is 1.05 \AA , the interlayer distance between bcc Fe and Fe_3O_4 is approximately 1.65 \AA , which is shorter than the distance $d \sim 2\text{ \AA}$ calculated for the B-Fe models I and II, as shown in Sec. III C. This result may be attributed to a sparse arrangement of Fe atoms on the A-Fe layer.

The lowest energy is -178.82 eV per unit cell, and P alignment is more stable than AP alignment. The energy difference, which is the EC energy $\Delta E = 0.16\text{ eV}$ per unit cell or 78 erg/cm^2 , is larger than the experimental value by two orders of magnitude. Both magnetization alignment and EC energy are thus in contradiction with the experimental results.

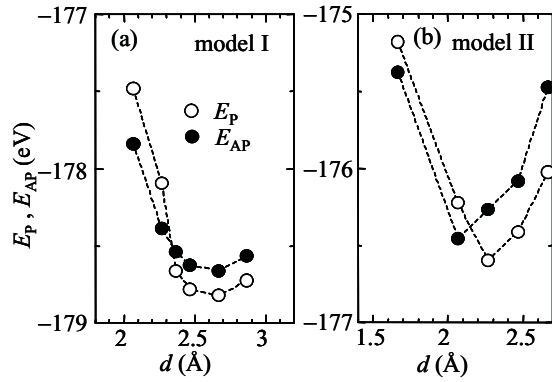


FIG. 6. Calculated results of total energy with parallel (P) and antiparallel (AP) alignments of bcc Fe and Fe_3O_4 magnetizations as a function of the interlayer distance between bcc Fe and B-Fe layers defined in Fig. 3. Results are for (a) A-Fe model I and (b) A-Fe model II. Open and closed symbols denote results for P and AP alignments of Fe and Fe_3O_4 magnetizations, respectively.

C. Results for bcc Fe/ Fe_3O_4 junctions with B-Fe layer termination

Figure 7 shows the calculated results for the local DOS of bcc Fe atoms and B-Fe ions at the interface of Fe/ Fe_3O_4 junctions with a B-Fe termination model I. The tendency of the change in the local DOS is almost the same as that shown in Fig. 5 for Fe/ Fe_3O_4 junctions with an A-Fe termination. The local DOS of B-Fe ions, however, is more distorted than that of A-Fe ions, and the energy band gap in the minority spin state completely disappears.

Table II shows the calculated results for m , which are also similar to those shown in Table I, except for one small difference. The magnetic moment of B-Fe ions on the atomic layer four is reduced to a lesser extent compared to that of A-Fe ions on the layer four in the structure of A-Fe models I and II. This result indicates that the magnetic moment of A-Fe ions is sensitive to perturbations caused by surrounding atoms.

The total energy of the junction is presented in Fig. 8 as a function of the interlayer distance d . The local minimum of the total energy appears at around $d = 2 \text{ \AA}$, which is relatively

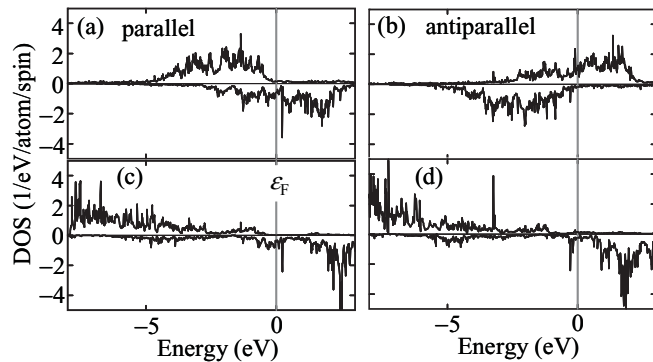


FIG. 7. (a) Local DOS of bcc Fe atoms at the interface in P alignment, and (b) those in AP alignment calculated for B-Fe model I. (c) Calculated results of local DOS of B-Fe ions at the interface of Fe_3O_4 layer in P alignment, and (d) those in AP alignment.

TABLE II. Calculated results for m on Fe atoms or ions in the unit cell in bcc Fe/ Fe_3O_4 junctions with B-Fe termination.

	L	I-P	I-AP	II-P	II-AP
bcc Fe	7	2.928	-2.931	2.925	-2.920
	7	2.926	-2.931	2.929	-2.920
	7	2.926	-2.931	2.924	-2.924
	7	2.928	-2.931	2.932	-2.921
	6	2.389	-2.405	2.370	-2.393
	6	2.346	-2.363	2.373	-2.387
	6	2.395	-2.423	2.373	-2.387
	6	2.326	-2.380	2.370	-2.393
	5	2.861	-2.817	2.745	-2.587
	5	2.862	-2.815	3.006	-2.995
B-Fe	4	3.792	3.824	3.926	3.914
	4	3.792	3.824	3.926	3.914
A-Fe	3	-4.048	-4.079	-4.040	-4.073
B-Fe	2	4.016	3.875	3.860	3.875
	2	4.016	3.875	3.860	3.875
A-Fe	1	-3.661	-3.647	-3.608	-3.647

larger than the interlayer distances 1.05 \AA in Fe_3O_4 and 1.48 \AA in bcc Fe. The large value of d may be attributed to the large ionic radius of O. Note that the size of the circles shown in the Fig. 3 corresponds to the ionic radii of Fe and O. The lowest energy state occurs in P alignment, similar to the calculated results for Fe/ Fe_3O_4 junctions with A-Fe termination. The lowest energy is -188.5 eV per unit cell. The values of ΔE are 0.11 eV per unit cell (52 erg/cm^2) for model I and 0.34 eV per unit cell (167 erg/cm^2) for model II, which are larger than the experimental value 1.5 erg/cm^2 by two orders of magnitude. The results are similar to those for junctions with A-Fe termination.

D. Relaxation of Fe atoms at interface

Thus far we have performed calculations for epitaxial Fe/ Fe_3O_4 junctions with flat interfaces. In real junctions, the interface cannot be perfectly flat and may include some roughness or disordered arrangement of atoms or ions. Although

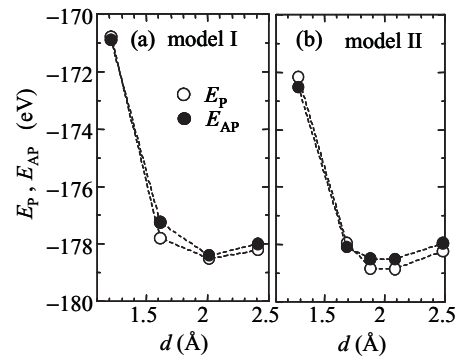


FIG. 8. Calculated results of E_P and E_{AP} for structures with (a) B-Fe termination with model I and (b) B-Fe termination with model II as a function of the interatomic distance d defined in Fig. 3.

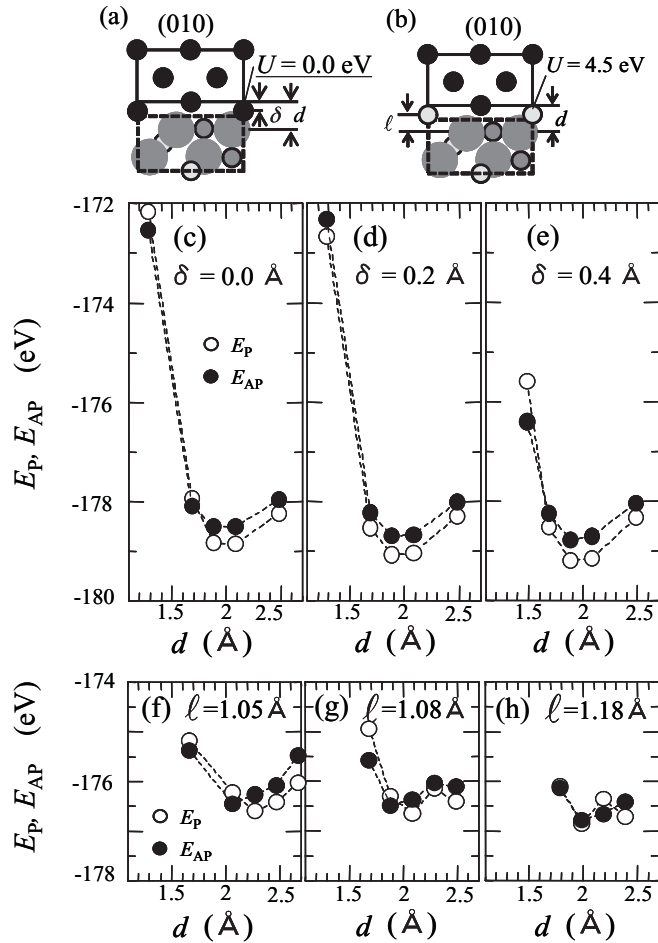


FIG. 9. (a) Lattice structure of unit cell in which Fe atoms of bcc Fe layer are relaxed and (b) in which A-Fe ions in Fe_3O_4 layer are relaxed. (c)–(e) Calculated results of total energy for P and AP alignments of magnetization as functions of distance d for several values of displacement δ of Fe atoms shown in (a). (f)–(h) Calculated results of total energy for displacement ℓ of A-Fe ions shown in (b).

there are many possible arrangements for disordered atoms, here we focus on the fact that the structure of B-Fe model II [see Fig. 3(b)] continuously changes into that of the A-Fe model II see Fig. 3(d)] by shifting the position of Fe atoms at the interface. Considering this fact, we performed first-principles calculations for the modified structures of B-Fe model II and A-Fe model II shown in Figs. 9(a) and 9(b), respectively. In the former structure, Fe atoms in the bcc Fe layer are shifted by a distance δ , and in the latter structure, A-Fe ions at the interface are shifted by ℓ . Note that the value of U is assumed to be zero for bcc Fe atoms but 4.5 eV for A-Fe ions for the structures shown in Figs. 9(a) and 9(b).

Calculated results for the total energy are shown in Figs. 9(c)–9(h) as a function of the interlayer distance d . Results with $\delta = 0$ and $\ell = 1.05$ Å shown in Figs. 9(c) and 9(f), respectively, are for unrelaxed structures. With increasing δ and ℓ , the lowest energy for E_P decreases. The interlayer distance d at which E_P is minimal seems to decrease with increasing δ or ℓ . The changes in E_P and d indicate that the structure tightens by relaxing Fe atoms at the interface.

The value of $\Delta E = E_{AP} - E_P$, however, remains positive irrespective of the shift in δ and ℓ , i.e., the P alignment of Fe and Fe_3O_4 magnetizations is stable. The magnitude of ΔE at $d = 2$ Å, shown in Fig. 9(h), is relatively small, but the dependence of ΔE on d seems to be less reliable in this case, possibly because of our treatment of U , which we assign as zero for Fe atoms in the bcc Fe layer and as 4.5 eV for A-Fe atoms in Fe_3O_4 . We find no stable AP alignment of bcc Fe and Fe_3O_4 magnetizations even for structures with relaxed Fe atoms or ions at the interface.

Fonin *et al.* observed a shift of B-Fe atoms ± 0.09 Å in the surface reconstruction.³¹ In our calculation, we did not consider such a lattice relaxation along lateral directions because a larger unit cell is required to include lattice relaxation along lateral directions. Judging from the results shown in Fig. 9, we expect that a lattice relaxation less than 0.1 Å may not change the sign of EC.

E. Relaxation of magnetic moment and value of U

The stability of AP alignment may be realized when the direction of the magnetic moments of atoms or ions at the interface is relaxed. Figures 10(a) and 10(b) show calculated results of E_P and E_{AP} as functions of the interlayer distance d for junctions with reversed magnetic moments on A-Fe layers at the interface and for those with reversed magnetic moments on bcc Fe atoms at the interface, respectively. The lattice structure shown in the inset is the same as that shown in Fig. 9(a) with $\delta = 0.4$ Å. The stable alignment is unchanged when the magnetic moment on the A-Fe layer is reversed, as shown in Fig. 10(a). However, in the structure shown in the inset of Fig. 10(b), AP alignment is stable at $d \sim 2$ Å. This result may suggest that a spatial fluctuation of the direction of magnetic moments may stabilize AP alignment of the magnetizations.

Here we perform GGA+ U calculations with small values of U , and examine effects of U on EC in Fe/ Fe_3O_4 . As for bulk properties of Fe_3O_4 , we obtain the half-metallic feature even for $U = 0$ with magnetic moments -3.4 and $3.5 \mu_B/\text{atom}$ for A-Fe and B-Fe, respectively. The results are similar to those calculated by Wenzel *et al.*⁴³ When the value of U is increased

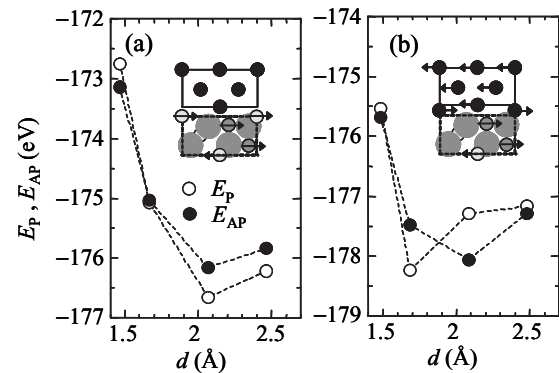


FIG. 10. Calculated results of E_P and E_{AP} for junctions with reversed magnetic moments on (a) A-Fe layer at the interface and (b) bcc Fe atoms at the interface with $\delta = 0.4$ Å as a function of the interlayer distance d . Open and closed circles indicate E_P and E_{AP} , respectively. Insets show the structure of the unit cell.

to 4 eV, the magnitude of the magnetic moments of A-Fe and B-Fe increased to be -4.0 and $3.9 \mu_B/\text{atom}$, respectively, and the energy band gap becomes larger than that calculated for $U = 0$. The large energy band gap is similar to that calculated by other groups^{41,42} and that calculated in HSE06 method,⁴⁶ but differs from that obtained by Wenzel *et al.*⁴³ At the present we do not understand the reason for the difference.

We have performed the calculation of ΔE with smaller values of U using larger k -point sampling (11,11,3) at the distance with the minimum energy shown in Figs. 6 and 8. The calculated values of ΔE for A-Fe model II, B-Fe model I, and B-Fe model II with $U = 3$ and 2 eV are 0.2–0.25 eV/unit cell, which are smaller than $\Delta E = 0.3$ –0.4 eV/unit cell calculated with $U = 4.5$ eV but are still positive. On the other hand, ΔE calculated for A-Fe model I are -0.007 and -0.180 eV/unit cell for $U = 3$ and 2 eV, respectively, showing a sign change as compared to the value of $\Delta E = 0.15$ eV/unit cell calculated for A-Fe model I with $U = 4.5$ eV.

A possible reason of the small/negative values of ΔE for A-Fe model I might be the following. As the value of U decreases, electrons on A-Fe sites may delocalize, and the overlap of the wave functions between bcc Fe and A-Fe sites becomes larger, resulting in a ferromagnetic coupling between bcc Fe and A-Fe atoms. Since the direction of magnetic moments on A-Fe is opposite to that of bulk magnetic moment, the exchange coupling between bcc Fe and Fe_3O_4 becomes AP. It may be noted that the distance between the nearest-neighbor A-Fe and bcc Fe atoms in this A-Fe model I is shorter than that in A-Fe model II. The result might suggest an importance of the choice of U at the interface.

IV. DISCUSSIONS

As presented in the previous section, the calculated EC energy ΔE equals 0.1–0.3 eV per unit cell and P alignment is stable in all the junction structures studied by using $U = 4.5$ eV. Furthermore, the absolute value of ΔE is relatively larger than the experimental value. Here, we first evaluate the magnitude of the exchange interaction from the value of ΔE by assuming that localized spins exist on Fe atoms or ions at the interface. Because the effective number of bonds of the exchange interaction can be approximately 10 and the magnitude of the localized spins is 1–2, the interaction constant can be of the order of 10 meV. This value is reasonable compared to the Curie temperature 10^3 K of bcc Fe and Fe_3O_4 .

Thus we conclude that the calculated EC energy corresponds to the exchange interactions at the flat interface and that the observed small EC must be explained by considering certain extrinsic mechanisms. We note here that the small value of ΔE calculated for A-Fe model I with $U = 3$ eV does not necessarily explain the observed EC, because our Mössbauer study, described below suggests that the B-Fe layer not the A-Fe layer contacts with the bcc Fe layer. One possible extrinsic mechanism is fluctuation or frustration effect on the EC as introduced for the IEC in magnetic multilayers,^{49–51} and another might be effects of excess oxidation at the interface of $\text{Fe}/\text{Fe}_3\text{O}_4$. In the following, we first discuss the effects of fluctuation/frustration and then examine a possibility of formation of negative moments of bcc Fe atoms at the interface due to excess oxidation. We consider the latter

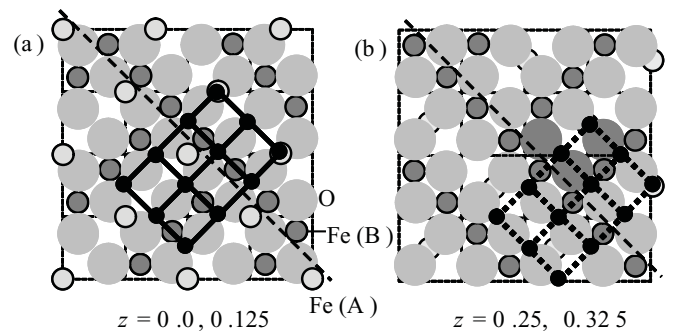


FIG. 11. Atomic arrangement of bcc Fe lattice (solid and broken lines) on Fe_3O_4 with antiphase structures. (a) Symbols show atomic positions in Fe_3O_4 with $z = 0.0$ and 0.125 layers, and (b) with $z = 0.25$ and 0.375 layers.

possibility because the first-principles calculation given in Sec. III-E indicates that the AP coupling could occur when negative moments of bcc Fe atoms at the interface are realized. Comparing results obtained in the first-principles and model calculations we propose a possible mechanism for the AP alignment.

We first show that an antiphase structure observed in thin Fe_3O_4 films⁵² could be responsible for the frustration of EC in $\text{Fe}/\text{Fe}_3\text{O}_4$ junctions. The antiphase structure proposed by Margulies *et al.*⁵² is shown in Figs. 11(a) and 11(b), where layers with $z = 0.0$ (0.25) and 0.125 (0.375) in Fig. 11(a) [see Fig. 11(b)] correspond to A-Fe and B-Fe layers, respectively. An antiphase boundary exists along the diagonal of the structure. When the bcc Fe lattice is placed on the layer with $z = 0.0$, as shown by solid lines in the figure, the contact structure is A-Fe model I for one phase and A-Fe model II for the other phase. When the bcc Fe lattice is placed on the layer with $z = 0.25$, as shown in Fig. 11(b) by broken lines, the contact structure is either B-Fe model I or B-Fe model II. In any case, the layer structure can be epitaxial without any lattice deformation. Because the magnetic coupling between the two phases of Fe_3O_4 is antiferromagnetic⁵² and the calculated EC gives P alignment between bcc Fe and Fe_3O_4 magnetizations, a frustration of the magnetic coupling appears.

A fluctuation in EC might also occur when B-Fe model II and A-Fe model II structures coexist with a constant interlayer distance d . As shown in Figs. 9(c) and 9(f), when $d \sim 2 \text{ \AA}$, P alignment in A-Fe model II and AP alignment in B-Fe model II coexist. This tendency exists even when the position of Fe atoms is allowed to relax at the interface. As presented in Fig. 10(b), AP alignment becomes stable when the magnetic moments of bcc Fe atoms are reversed at the interface. This could be another source of fluctuation or frustration in EC. Coexistence of B-Fe models and A-Fe model I might also give rise to a frustration when a small value of U is realized at the interface.

Now we study EC adopting a simple one-dimensional single-orbital tight-binding model with the assumption that the interface of $\text{Fe}/\text{Fe}_3\text{O}_4$ junctions is insulating. This assumption is justified by a recent experiment on the electrical resistance of $\text{Fe}/\text{Fe}_3\text{O}_4$ junctions.⁵³

Figure 12(a) shows a schematic of the structure of a model junction in which an impurity is located at site i . The left chain

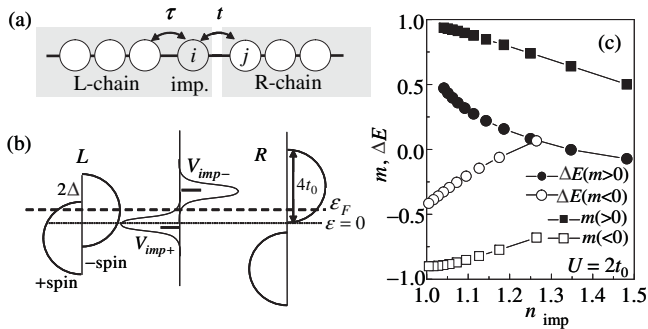


FIG. 12. One-dimensional model based on a single-orbital tight-binding model. (a) Schematic of the model. (b) Schematic of the DOS of L- and R-chains and an impurity. (c) Results of magnetic moments m ($\mu_B/\text{atom} \times \text{orbital}$) and ΔE (arb. unit) calculated self-consistently as a function of electron number n_{imp} ($1/\text{atom} \times \text{orbital}$) on the impurity.

(L-chain) and right chain (R-chain) correspond to bcc Fe and Fe_3O_4 layers, respectively. The hopping parameter is t_0 in both chains. In the one-dimensional model, the bandwidth of each spin state is $4t_0$. The hopping integral between the L chain and impurity is assumed to be $\tau = 0.5t_0$. The hopping integral t between sites i and j is treated as a perturbation up to t^2 in the formalism for ΔE (see Appendix). Figure 12(b) shows a schematic of the DOS of L and R chains and the impurity site; R-DOS is assumed to be half-metallic. To determine the magnetic state of the impurity, we introduce an onsite Coulomb interaction U , and apply the Hartree-Fock approximation to the interaction. As a result, the onsite potential at the impurity is given as $V_{imp\sigma} = V_{imp0} + Un_{imp-\sigma}$, where V_{imp0} is the bare energy level of the impurity and $n_{imp\sigma}$ is the number of electrons at the impurity with spin σ . The values of $n_{imp\sigma}$ are self-consistently calculated for various values of V_{imp0} . Figure 12(c) shows the magnetic moment of the impurity $m = n_{imp\uparrow} - n_{imp\downarrow}$ and ΔE as a function of the electron number on the impurity site $n_{imp} = n_{imp\uparrow} + n_{imp\downarrow}$. We observe that a solution with $m < 0$ appears for small values of n_{imp} , and that ΔE becomes negative when $m < 0$.

We may also model an A-Fe ion by the Fe_3O_4 layer as a nearly localized impurity by R-chain. For this case, we confirmed the magnetic state of the impurity does not affect the sign of ΔE . This is because the impurity state is strongly exchange-split by the Coulomb interaction and produce no state near the Fermi energy. The results are similar to those calculated in the first principles shown in Fig. 10(a).

Thus, we expect that when Fe atoms at the interface of the bcc Fe layer are highly oxidized, the d orbitals of Fe ions are nearly half-filled and the direction of their magnetic moments can be opposite to that in the bcc Fe layer, resulting in AP alignment of bcc Fe and Fe_3O_4 magnetization. To examine the result, we have performed two first-principles calculations for A-Fe model II with $U = 4.5$ eV including excess oxygen; in one calculation A-type Fe atoms at the interface are replaced with O atoms, and in the other calculation one bcc Fe atom in the unit cell at the interface is replaced with one O atom. The energy difference ΔE decreased by 60 and 30% for the former and latter calculations, respectively, but they are still positive.

The oxygen excess, however, shows a tendency to make the coupling AP.

Dependence of the magnetic moment on number of electrons on Fe ions may predict the following: when Fe atoms are replaced with Co atoms in the bcc Fe layer, the P alignment should become more stable because the number of electrons in Co atoms is larger than that of Fe atoms by 1/atom. On the other hand, when Cr or Mn atoms are replaced with Fe atoms, the AP alignment should become stronger.

In addition to P and AP alignment, a noncollinear alignment of magnetic moments could possibly appear at local regions with magnetic frustrations. Such a noncollinear alignment, however, may not be realized in the present first-principles calculation for clean interfaces because the coupling between magnetic moments has been found to be strong in the present calculations.

A nonuniform magnetic state that possibly exists at the interface of Fe/ Fe_3O_4 junctions can be studied by using Mössbauer spectroscopy for samples containing ^{57}Fe isotopes only at the interface.⁴⁴ Preliminary results are available for two samples in which ^{57}Fe is introduced into the interface of either the bcc Fe or Fe_3O_4 layers with about one atomic layer. Based on the hyperfine field obtained from the analysis of the Mössbauer spectra, we suggest that Fe_3O_4 layer is terminated by a B-Fe layer and that the hyperfine field is enhanced in the atomic layers at the interface of the Fe layer. The enhancement of the hyperfine field possibly originates from the random oxidation of Fe atoms at the interface. As mentioned in Sec. III D, Fe ions in B-Fe model II and A-Fe model II can be continuously distributed at the interface. Therefore depending on the degree of oxidation, these Fe ions can have either A-Fe or bcc Fe character, which may result in the enhancement of the hyperfine field. More detailed experiments are in progress.

V. CONCLUDING REMARKS

We have performed first-principles band calculations to study the electronic and magnetic states of Fe/ Fe_3O_4 junctions and to clarify the mechanism behind EC in Fe/ Fe_3O_4 junctions. These calculations were performed for four types of the unit cells with epitaxial stacking of the bcc Fe on Fe_3O_4 layer. The relaxation of Fe atoms or ions at the interface has also been considered.

We proved that the magnitude of the local Fe moments at the interface increases for Fe in bcc Fe layers, but decreases for Fe in Fe_3O_4 layers. By plotting the total energy of the junctions in both P and AP magnetization alignments as a function of the interlayer distance between Fe and Fe_3O_4 layers, we obtain the EC energy of the junctions. Calculated results for the coupling energy, however, are larger than the experimental results by two orders of magnitude and may not correspond to the observed EC energy but rather to the exchange interaction between near-neighbor spins on Fe atoms or ions.

The detailed study in the first-principles calculation indicates the importance of the magnetic state at the interface; delocalization/localization of electrons and oxidation by excess oxygen at the interface, and that the origin of the AP magnetization alignment reported in experiments may be of extrinsic origin rather than of intrinsic origin at clean interfaces. To explain the experimental results, we have combined the results

obtained in the first-principles calculations with those in a model calculation, and proposed a plausible mechanism of AP alignment in which EC is mediated by impurity-like states of Fe atoms that possess magnetic moments aligned opposite to those in the bcc Fe layer. The impurity mediated EC may produce AP alignment when the intrinsic EC between flat interface is suppressed by frustration effects or formation of an insulating interface. We further propose that substitution of Fe atoms at the bcc Fe interface with Co (Cr, Mn) may decrease (increase) the antiparallel coupling between bcc Fe and Fe₃O₄ magnetizations. In this way experiments will easily confirm the mechanism proposed above by doping various types of impurities at the interface. Because the proposed mechanism may be realized in complicated structures at interfaces with additional oxidation, first-principles study of the extrinsic mechanism may be a research in near future.

ACKNOWLEDGMENTS

This work was supported by Elements Science and Technology Projects of MEXT, Japan. JI appreciates a Grant-in-Aid for Scientific Research in Priority Area “Creation and control of spin current” from MEXT, Japan, and the Next-Generation Supercomputing Project, Nanoscience Program, MEXT, Japan for partial support.

APPENDIX

The coupling energy of junctions is calculated using a hopping parameter t , shown in Fig. 12(a), as a perturbation via the following procedure. Letting $\mathbf{G}(\varepsilon)$ be a Green’s function of the system, the total energy of the system is

$$E = -\frac{1}{\pi} \int_{-\infty}^{\varepsilon_F} \text{Im Tr} \ln \mathbf{G}(\varepsilon) d\varepsilon. \quad (\text{A1})$$

When the perturbation Hamiltonian is written as \mathbf{V} and the unperturbed Green’s function as $\mathbf{g}(\varepsilon)$, $\mathbf{G}(\varepsilon) = \mathbf{g}(\varepsilon)[1 -$

$\mathbf{V}\mathbf{g}(\varepsilon)]^{-1}$. Therefore the total energy is divided into two parts:

$$E = E_0 + \delta E, \quad (\text{A2})$$

$$E_0 = -\frac{1}{\pi} \int_{-\infty}^{\varepsilon_F} \text{Im Tr} \ln \mathbf{g}(\varepsilon) d\varepsilon, \quad (\text{A3})$$

$$\delta E = \frac{1}{\pi} \int_{-\infty}^{\varepsilon_F} \text{Im Tr} \ln [1 - \mathbf{V}\mathbf{g}(\varepsilon)] d\varepsilon. \quad (\text{A4})$$

Here, \mathbf{V} corresponds to the hopping parameter t between two semi-infinite metals, E_0 is the energy of a system containing two independent metals, and δE is the energy change caused by introducing t , i.e., the coupling energy of the two metals. Expanding $\ln[1 - \mathbf{V}\mathbf{g}(\varepsilon)]$ with respect to $V = t$ up to the second-order term, we obtain

$$\delta E = -\frac{t^2}{2\pi} \sum_{\sigma} \int_{-\infty}^{\varepsilon_F} \text{Im}[g_{i\sigma}(\varepsilon)g_{j\sigma}(\varepsilon)] d\varepsilon, \quad (\text{A5})$$

where i and j are the site indices shown in Fig. 12(a). Here, the summation over spin σ is explicitly introduced. A term linear to t vanishes when the trace is adopted. The EC energy corresponds to the EC constant J defined as

$$J = dE_P - dE_{AP}, \quad (\text{A6})$$

with

$$\delta E_{P(AP)} = -\frac{t^2}{\pi} \int_{-\infty}^{\varepsilon_F} \text{Im}[g_{i+}(\varepsilon)g_{j+(-)}(\varepsilon) \quad (\text{A7})$$

$$+ g_{i-}(\varepsilon)g_{j-(+)}(\varepsilon)] d\varepsilon, \quad (\text{A8})$$

where $+$ and $-$ indicate the majority and minority spin states, respectively.⁵⁴ The local Green’s functions are easily calculated for one-dimensional systems. The present formalism of the EC has already been adopted for IEC in magnetic multilayers,⁵⁵ but the Hamiltonian in the present formalism, which is perturbed by the hopping parameter between two layers, is slightly different from the choice adopted for IEC in magnetic multilayers.

*inoue@nuap.nagoya-u.ac.jp

¹P. Grünberg, R. Schreiber, Y. Pang, M. B. Brodsky, and H. Sowers, *Phys. Rev. Lett.* **57**, 2442 (1986).

²M. N. Baibich, J. M. Broto, A. Fert, F. Nguyen Van Dau, F. Petroff, P. Etienne, G. Creuzet, A. Friederich, and J. Chazelas, *Phys. Rev. Lett.* **61**, 2472 (1988).

³S. S. P. Parkin, N. More, and K. P. Roche, *Phys. Rev. Lett.* **64**, 2304 (1990).

⁴S. S. P. Parkin, *Phys. Rev. Lett.* **67**, 3598 (1991).

⁵T. Miyazaki and N. Tezuka, *J. Magn. Magn. Mater.* **139**, L231 (1995).

⁶J. S. Moodera, L. R. Kinder, T. M. Wong, and R. Meservey, *Phys. Rev. Lett.* **74**, 3273 (1995).

⁷W. H. Meiklejohn and C. P. Bean, *Phys. Rev.* **102**, 1413 (1956).

⁸F. Radu and H. Zabel, *STMP* **227**, *Magnetic Heterostructures*, edited by H. Zabel and S. D. Bader, 97 (2008).

⁹R. A. de Groot, F. M. Mueller, P. G. van Engen, and K. H. J. Buschow, *Phys. Rev. Lett.* **50**, 2024 (1983).

¹⁰E. O. Wollan and W. C. Koehler, *Phys. Rev.* **100**, 545 (1955).

¹¹P.-G. de Gennes, *Phys. Rev.* **118**, 141 (1960).

¹²*Colossal Magnetoresistive Oxides*, edited by Y. Tokura (Gordon and Breach, NY, 2000).

¹³Y. Sakuraba, J. Nakata, M. Oogane, H. Kubota, Y. Ando, A. Sakuma, and T. Miyazaki, *Jpn. J. Appl. Phys.* **44**, L1100 (2005).

¹⁴T. Marukame, T. Ishikawa, S. Hatamata, K. Matsuda, T. Uemura, and M. Yamamoto, *Appl. Phys. Lett.* **90**, 012508 (2007).

¹⁵A. Yanase and K. Shiratou, *J. Phys. Soc. Jpn.* **53**, 312 (1984).

¹⁶Z. Zhang and S. Satpathy, *Phys. Rev. B* **44**, 13319 (1991).

¹⁷X. W. Li, A. Gupta, G. Xiao, W. Qian, and V. P. Dravid, *Appl. Phys. Lett.* **73**, 3282 (1998).

¹⁸P. Seneor, A. Fert, J.-L. Maurice, F. Montaigne, F. Petroff, and A. Vaures, *Appl. Phys. Lett.* **74**, 4017 (1999).

- ¹⁹H. Matsuda, M. Takeuchi, H. Adachi, M. Hiramoto, N. Matsukawa, A. Odagawa, K. Setsune, and H. Sakakima, *Jpn. J. Appl. Phys., Part 2* **41**, L387 (2002).
- ²⁰G. Hu and Y. Suzuki, *Phys. Rev. Lett.* **89**, 276601 (2002).
- ²¹M. G. Chapline and S. X. Wang, *Phys. Rev. B* **74**, 014418 (2006).
- ²²E. Weal, S. Patnaik, Z. Bi, H. Wang, T. Fix, A. Kursumovic, and J. L. MacManus Driscoll, *Appl. Phys. Lett.* **97**, 153121 (2010).
- ²³Yan Li, Wei Han, A. G. Swartz, K. Pi, J. J. I. Wong, S. Mack, D. D. Awschalom, and R. K. Kawakami, *Phys. Rev. Lett.* **105**, 167203 (2010).
- ²⁴H. Yanagihara, Y. Toyoda, and E. Kita, *J. Appl. Phys.* **101**, 09D101 (2007).
- ²⁵H. Yanagihara, Y. Toyoda, A. Ohnishi, and E. Kita, *Appl. Phys. Exp.* **1**, 111303 (2008).
- ²⁶H. Yanagihara, Y. Toyoda, and E. Kita, *J. Phys. D: Appl. Phys.* **44** (2011).
- ²⁷J. C. Slonczewski, *Phys. Rev. B* **39**, 6995 (1989).
- ²⁸P. Bruno, *Phys. Rev. B* **49**, 13231 (1994).
- ²⁹J. Faure-Vincent, C. Tiusan, C. Bellouard, E. Popova, M. Hehn, F. Montaigne, and A. Schuhl, *Phys. Rev. Lett.* **89**, 107206 (2002).
- ³⁰T. Katayama, S. Yuasa, J. Velev, M. Ye Zhuravlev, S. S. Jaswal, and E. Y. Tsybal, *Appl. Phys. Lett.* **89**, 112503 (2006).
- ³¹M. Fonin, R. Pentcheva, Yu. S. Dedkov, M. Sperlich, D. V. Vyalikh, M. Scheffler, U. Rudiger, and G. Guntherodt, *Phys. Rev. B* **72**, 104436 (2005).
- ³²R. Pentcheva, F. Wendler, H. L. Meyerheim, W. Moritz, N. Jedrecy, and M. Scheffler, *Phys. Rev. Lett.* **94**, 126101 (2005).
- ³³R. Pentcheva, W. Moritz, J. Rundgren, S. Frank, D. Schrupp, and M. Scheffler, *Surf. Sci.* **602**, 1299 (2008).
- ³⁴E. J. W. Verwey and P. W. Haaymann, *Physica* **8**, 979 (1941).
- ³⁵E. J. W. Verwey and E. L. Heilmann, *J. Phys. Chem.* **15**, 174 (1947).
- ³⁶J. P. Wright, J. P. Attfield, and P. G. Radaelli, *Phys. Rev. Lett.* **87**, 266401 (2001).
- ³⁷V. I. Anisimov, I. S. Elfimov, N. Hamada, and K. Terakura, *Phys. Rev. B* **54**, 4387 (1996).
- ³⁸V. N. Antonov, B. N. Harmon, V. P. Antropov, A. Ya. Perlov, and A. N. Yaresko, *Phys. Rev. B* **64**, 134410 (2001).
- ³⁹V. N. Antonov, B. N. Harmon, and A. N. Yaresko, *Phys. Rev. B* **67**, 024417 (2003).
- ⁴⁰I. Leonov, A. N. Yaresko, V. N. Antonov, M. A. Korotin, and V. I. Anisimov, *Phys. Rev. Lett.* **93**, 146404 (2004).
- ⁴¹H-T. Jeng, G. Y. Guo, and D. J. Huang, *Phys. Rev. Lett.* **93**, 156403 (2004).
- ⁴²Z. Szotek, W. M. Temmerman, D. Ködderitzsch, A. Svane, L. Petit, and H. Winter, *Phys. Rev. B* **74**, 174431 (2006).
- ⁴³M. J. Wenzel and G. Steinle-Neumann, *Phys. Rev. B* **75**, 214430 (2007).
- ⁴⁴K. Mibu *et al.* (unpublished).
- ⁴⁵G. Kresse and D. Joubert, *Phys. Rev. B* **59**, 1758 (1999).
- ⁴⁶J. Heyd, G. E. Scuseria, and M. Ernzerhof, *J. Chem. Phys.* **124**, 219906 (2006).
- ⁴⁷V. C. Rakhecha and N. S. Satya Murthy, *J. Phys. C* **11**, 4389 (1978).
- ⁴⁸A. Claassen, *Proc. Phys. Soc.* **38**, 482 (1925-26).
- ⁴⁹B. Heinrich, *STMP* **227**, *Magnetic Heterostructures*, edited by H. Zabel and S. D. Bader, 185 (2008).
- ⁵⁰W. Kakeno, S. Honda, J. Inoue, and H. Itoh, *J. Magn. Soc. Jpn.* **34**, 92 (2010).
- ⁵¹W. Kakeno, S. Honda, H. Itoh, and J. Inoue, *Phys. Rev. B* **82**, 014413 (2010).
- ⁵²D. T. Margulies, F. T. Parker, M. L. Rudee, F. E. Spada, J. N. Chapman, P. R. Aitchison, and A. E. Berkowitz, *Phys. Rev. Lett.* **79**, 5162 (1997).
- ⁵³H. Yanagihara *et al.* (unpublished).
- ⁵⁴D. M. Edwards, A. M. Robinson, and J. Mathon, *J. Magn. Magn. Mater.* **140-144**, 517 (1995).
- ⁵⁵J. d'Albuquerque e Castro, J. Mathon, M. Villeret, and A. Umerski, *Phys. Rev. B* **53**, R13306 (1996).